TECHNICAL REPORT
NATICK/TR-15/019

AD _____

PHOTOVOLTAIC FABRICS

by
Paul Calvert
Russ Gaudiana*
Yong Kim
Richard Childress*
Michael Lee*
Joseph Mayer
and
Dapeng Li

University of Massachusetts – Dartmouth
Dartmouth, MA 02747-2300

***Lowell Consulting Group**
Lowell, MA 01852

April 2015

Final Report
February 2013 – October 2014

Approved for public release; distribution is unlimited

Prepared for
U.S. Army Natick Soldier Research, Development and Engineering Center
Natick, Massachusetts 01760-5020

DISCLAIMERS

The findings contained in this report are not to be construed as an official Department of the Army position unless so designated by other authorized documents.

Citation of trade names in this report does not constitute an official endorsement or approval of the use of such items.

DESTRUCTION NOTICE

For Classified Documents:

Follow the procedures in DoD 5200.22-M, Industrial Security Manual, Section II-19 or DoD 5200.1-R, Information Security Program Regulation, Chapter IX.

For Unclassified/Limited Distribution Documents:

Destroy by any method that prevents disclosure of contents or reconstruction of the document.

REPORT DOCUMENTATION PAGE

Form Approved
OMB No. 0704-0188

PLEASE DO NOT RETURN YOUR FORM TO THE ABOVE ADDRESS.

1. REPORT DATE *(DD-MM-YYYY)*	2. REPORT TYPE	3. DATES COVERED *(From - To)*
22-04-2015	Final Report	February 2013 – October 2014

4. TITLE AND SUBTITLE

PHOTOVOLTAIC FABRICS

5a. CONTRACT NUMBER
W911QY-13-C-0018

5b. GRANT NUMBER

5c. PROGRAM ELEMENT NUMBER
622786/E01

6. AUTHOR(S)

Paul Calvert, Russ Gaudiana*, Yong Kim, Richard Childress*, Michael Lee*, Joseph Mayer and Dapeng Li

5d. PROJECT NUMBER

5e. TASK NUMBER

5f. WORK UNIT NUMBER

7. PERFORMING ORGANIZATION NAME(S) AND ADDRESS(ES)

University of Massachusetts – Dartmouth
285 Old Westport Road
Dartmouth, MA 02747-2300

8. PERFORMING ORGANIZATION REPORT NUMBER

9. SPONSORING / MONITORING AGENCY NAME(S) AND ADDRESS(ES)

U.S. Army Natick Soldier Research, Development and Engineering Center
ATTN: RDNS-SEW-TMN (DeCristofano)
Kansas Street, Natick, MA 01760-5020

10. SPONSOR/MONITOR'S ACRONYM(S)
NSRDEC

11. SPONSOR/MONITOR'S REPORT NUMBER(S)
NATICK/TR-15/019

12. DISTRIBUTION / AVAILABILITY STATEMENT

Approved for public release; distribution is unlimited

13. SUPPLEMENTARY NOTES

* Lowell Consulting Group, 116 John St, Lowell, MA 01852

14. ABSTRACT

This report describes a project to improve photovoltaic fabrics. It had four objectives: 1) Efficiency – make PV wires on a continuous basis that exhibit 7% efficiency; 2) Automated Welding – demonstrate an automated means of interconnecting the electrodes of one wire to the electrodes of a neighboring wire; 3) Weaving – fabric to determine the optimum wire density, relative to the co-woven inert yarn, for power production, flexibility, and wearability; 4) Battery Charging - produce fabrics that are able to charge 4AA batteries within 4 hours of exposure to direct sunlight (AM1.5). Over the duration of the project we demonstrated PV efficiency ranging from 5.04% (wire on a black background) to >8% efficiency on a white cloth background. A bare primary electrode on a nano-silver coating exhibited an efficiency of 6.45%. This high level of performance was accomplished by means of high performance active layer polymers, stainless steel electrodes with lower resistivity, optimized coating formulations for all layers, a new cladding formulation, and process optimization. We supplied several thousand feet of high performance PV wire for weaving trials and fabric delivery.

15. SUBJECT TERMS

WIRE	DENSITY	PLASMONS	AUTOMATION	BATTERY CHARGERS
FIBERS	WEAVING	BATTERIES	WOVEN FABRICS	FLEXIBLE MATERIALS
ENERGY	WELDING	EFFICIENCY	PHOTOVOLTAICS	PHOTOVOLTAIC WIRES
LAYERS	FLEXIBLE	ELECTRODES	POLYESTER FIBERS	
FABRICS	CLADDING	SOLAR CELLS	PV(PHOTOVOLTAIC)	

16. SECURITY CLASSIFICATION OF:			17. LIMITATION OF ABSTRACT	18. NUMBER OF PAGES	19a. NAME OF RESPONSIBLE PERSON
a. REPORT	b. ABSTRACT	c. THIS PAGE			Barry DeCristofano
U	U	U	UU	48	19b. TELEPHONE NUMBER *(include area code)* (508) 233-4255

This page intentionally left blank

Table of Contents Page

List of Figures

List of Tables

PHOTOVOLTAIC FABRICS

Introduction

This report describes work to improve photovoltaic fabrics, performed from February 2013 to October 2014, under a contract (W911QY-13-C-0018) awarded to the University of Massachusetts – Dartmouth by the Natick Soldier Research, Development and Engineering Center (NSRDEC)..

The project had four Objectives:

1. *Efficiency* - make photovoltaic (PV) wires on a continuous basis that exhibit 7% efficiency;
2. *Automated Welding* - demonstrate an automated, mechanical means of interconnecting, e.g., welding, the electrodes of one wire to the electrodes of a neighboring wire;
3. *Weaving* – develop the ability to weave large areas (many square feet) of fabric on a hand loom to determine the optimum PV wire density (count) relative to the co-woven inert yarn that a fabric should have for power production, flexibility, and wearability (fit and feel);
4. *Battery Charging* - produce fabrics able to charge 4 AA batteries (2000 mAhr capacity) within 4 hours of exposure to direct sunlight (AM 1.5).

Over the duration of the project we demonstrated PV efficiency ranging from 5.04% (clad PV wire on a black background) to > 8% efficiency (PV wire on a white cloth background). A bare primary electrode on a nano-silver coating exhibited an efficiency of 6.45%. This high level of performance was accomplished by means of advanced, high performance active layer polymers, stainless steel electrodes with lower resistivity, optimized coating formulations for all layers, a new cladding formulation, and process optimization.

Furthermore, we supplied several thousand feet of high performance PV wire for weaving trials and fabric delivery.

When we terminated an earlier project in 2009, the major problem centered on our inability to weld PV wires in an automated process. A completely automated system must

comprise three functions. The first is stripping off the cladding. Both thermal mechanical stripping and solvent stripping of the cladding have been demonstrated, but neither has been automated. Second, a vision system that is capable of distinguishing the primary and secondary electrodes has been demonstrated and installed as part of a custom built welder. Third, a welding unit must be capable of welding of the primary or secondary electrode of one PV wire to either the primary or the secondary electrode of a neighboring wire. Automated welding with 100% repeatability has been demonstrated.

In regard to weaving, foot-wide, multi-yard long strips of fabric were woven on a computer-controlled loom with a hand-operated shuttle. Special fabrics were designed to ensure maximum exposure of the wires (> 80%) on the surface of the fabric to facilitate the welding process; these had a warp-free space close to one edge to allow the welder to operate in the space while the edge was clamped. Space free of the PV weft wire was left so that the PV sections could operate as discrete modules and could be cut and stitched as necessary. Methods for spooling the wire on the shuttles were developed to minimize twist build-up in the stiff PV wires. This was complemented by designs to reduce the degree of twist incorporated when the secondary electrode was wound during wire fabrication. Weaving was demonstrated for both military-type nylon-cotton blend (NYCO) warp fibers and cotton-polyester warp fibers. A number of different weave patterns were tested with various sateen structures where the weft floats over different numbers of warp fibers before going under one warp fiber and returning to the top surface thus producing maximum exposure of the PV wires in the weft. At the edges of the fabric, long loops were added to allow the fiber to relax before re-entering, so that they did not twist. These loops are eventually cut off after welding. The fabric produced was very flexible when bent in the weft direction, e.g., parallel to the wires, but somewhat stiff when bent in the warp direction.

Battery charging requires fabric that exhibits power and voltage that is a simple multiple of the individual cell power and voltage. Unfortunately, the current weaving process bends the wires comprising each cell at a very acute angle which creates shorts or partial shorts at every turn. As a result every cell exhibits either very low voltage, e.g., < 0.4 V, or is nearly dead, e.g., << 0.1 V; typically each cell exhibits > 0.5 V when not shorted. As a consequence of this problem, which surfaced at the end of the project, a demonstration of battery charging using these fabrics is not possible. This is not to suggest that the wires cannot be bent. We have

determined that when the wires are bent around a 1.5-mm-diameter post no shorts are found, and the wires exhibit the expected voltage and power. At the present time, the minimum bend diameter has not been determined.

Project Tasks – Summary and Results

Task 1 – New Active Layer Polymers

Using active layer polymer combinations first devised by Konarka Technologies, Inc., in combination with improved hole and electron injecting layers and more conductive electrode wires, we have achieved the efficiency target (6.45% for bare primary wire to 8.5% for clad wire on a white cloth).

Task 2 – Higher Index Wire Cladding

Many polymers and polymer blends, e.g., polystyrenes, acrylics, epoxides and titanates, were tried as candidates for high index claddings. Several of these materials exhibited refractive index values greater than 1.7. In addition, non-polymeric, organic and inorganic, index-enhancing additives were also tested in several cladding formulations. Several of these formulations exhibited the appropriate viscosity and rheological properties, as well as mechanical properties (e.g., flexibility and toughness) and optical properties (e.g., non-scattering and colorless), required for PV wire cladding. Unfortunately, the great majority of these cladding formulations caused degradation in PV performance. The best cladding formulations comprise Permabond (a commercially available UV curable formulation) and Perkalite (a plate-like clay at 15 wt%) with or without an index-enhancing additive (1.58 – 1.59 index at 15 wt%). Efficiency of the wire with the clay alone is enhanced by 10%, probably due to optical diffusion, and it is currently used as the cladding formulation for the wire.

Task 3- Develop a Light Harvesting Cladding

Sub-Tasks 3.1 – 3.4 – Plasmons

Difficulties were encountered with the plasmon formulations when attempting to incorporate them into the cladding formulation. Although the solvents comprising the plasmon formulation are compatible with the cladding, upon addition of the plasmon suspension to the cladding, the plasmons aggregated and precipitated. A considerable amount of additional research is required before a stable suspension of plasmons in the cladding can be generated and tested.

Sub-Task 3.5 – Fluorescent Dyes

Several commercially available dyes were individually incorporated into the cladding. None of these dyes improved the efficiency of the wire. Our modeling shows that the candidate dye must have an absorption band that has zero overlap with the absorption bands of the active layer polymer, and the emission band of the dye must coincide precisely with the absorption band of the active layer polymer.

Task 4 – New HIL Polymers

Several new commercially available hole-injection layer (HIL) materials were tested. They all exhibited improved PV performance but, with the exception of Clevious PH 1000, they all failed stability tests.

Task 5 – New Nano-particulate Silver Electrode

We made several nano-silver formulations and experimented with commercially available formulations as coatings on the silver-cored, stainless steel secondary electrode. The main problem with most of these is non-uniform coating due to curing of the polymer binder over time which means that long lengths of wire could not be produced. One exception is a nano-silver formulation supplied by UT Dots, Inc., which exhibited an improved fill factor essentially equal to that of plated silver on the secondary electrode.

Task 6 - Carbon Fiber Counter Electrode

When the proposal was written, we had been using stainless steel (SS) wire for both the primary and secondary electrodes. This wire is stiff and adds weight to the PV wire. Commercially available carbon fiber cord has a resistivity in the same range as that of stainless steel (138 Ω/cm for SS vs. 198 Ω/cm for carbon fiber) and it also has a very high modulus while exhibiting very good flexibility. Near the beginning of the current project we became aware that diamond-drawn, stainless steel with a silver core had become available. Its resistivity with a 30% silver core is 2.3 Ω/cm, and after annealing, it is more flexible than stainless steel wire. We used this silver-cored wire as the primary electrode with excellent results. When this wire was used as the secondary electrode, the performance was improved further. So, even though the carbon fiber was considered for use, in the end, it was not needed because a better material was available.

Task 7 – Wire Interconnects

A wire welding unit incorporating a vision system was designed and built.

1) Removing the cladding:

   We demonstrated that both thermal mechanical stripping and solvent stripping of the cladding spontaneously separates and spreads the primary and secondary electrodes, making them readily accessible. We have not attempted to automate the stripping process.

2) Distinguishing the primary from the secondary electrode:

   A vision system capable of distinguishing the two electrodes was installed as part of the welder.

3) Welding:

   We demonstrated an automated welding unit that is capable of welding the primary or secondary electrode of one PV wire to either the primary or the secondary electrode of its neighbor.

Task 8 – Weaving

The weaving process has been summarized above and has been reported in detail each month.

Fabrics were produced with about 70 ends per inch of NYCO warp yarn and 50 picks per inch of PV weft fiber. Textured polyester filament yarns were also used. Each yarn type had specific problems with breakage and tangling during weaving but these were resolved. Fabrics were made with 6, 8 and 12 harness patterns. 8 harnesses gives the greatest upper-surface exposure of the PV fibers and seems to be quite stable.

An end-loop pattern was settled on that gives 96 inches of PV fiber in series (6 passes through an 8-inch wide fabric) that is then welded in parallel along the edges to deliver 6 V from 12 lengths. These are then joined in series to form a power module 12 inches long. This structure is achieved by having tight loops along the right-hand side of the fabric and 5 picks of tight loops followed by one loose loop for welding along the left-hand side.

Test samples were made using an early version of the welding process for mechanical and optical testing. Optically (report 16), it was found that about 40% of the light was absorbed by the PV fibers, with the remainder being transmitted through the fabric or reflected.

Optimization of the optical properties of the fabric should allow this 40% value to be significantly increased.

Mechanically, compared to conventional uniform fabric, it was found that the PV fabric was half as stiff in the warp direction, that is when tested across the PV fibers. In the weft direction, when measured parallel to the PV fibers, the PV fabric was 6 times as stiff as conventional fabric made from NYCO yarns. Conventional fabric itself is twice as stiff in the weft direction than in the warp direction. Thus, as it stands, the PV fabric would not easily flex and conform to complex curvature, such as an armpit, but it is also unlikely that this would be needed.

As would be expected for metal wires tested in tension, the PV fabric also failed at low strains (1-2%) in the weft direction but withstood high strains (20%) in the warp direction. Tests of PV output were performed during cyclic strain with an early version of the welded wire. At about 1% cyclic strain positive and negative (buckling) in the weft direction the fabric performed well for about 50 cycles before the joints started to fail. Strain itself had little effect on the open circuit voltage output. Clearly a much more thorough test program would be needed but the initial studies suggest that cyclic stretching will not have a major impact on the fabric output.

Task 9 – Power Application

Battery charging was not possible because of issues with the woven fabric. Many of the cells within the fabric were damaged due to the small bend radius at the edge of the fabric. This resulted in significantly reduced electrical performance of each cell. For example, the open circuit voltage (V_{oc}) was as little as 0.096 V in the woven fabric, compared to the expected value of 0.55 V. We determined that the cause of the problem was indeed the bend radius by removing wires from the center of the fabric, between the bent ends. These wires performed as expected.

The specific cause of the problem is thought to be “micro-shorts” between the primary and secondary wires at the bend location. Essentially the secondary wire partially breaks through the OPV coating and touches the primary wire causing current leakage and significantly reduced voltage. These are not direct shorts that would reduce the voltage to zero, but compromised regions that dramatically reduce electrical performance.

There are solutions to the bend radius problem that can be easily incorporated into the weaving process. These include multiple shuttles to increase the spacing between wire ends and thus widen the bend radius of the wire loops at the fabric edge.

In an effort to understand battery charging performance of an undamaged fabric, a hand-made simulation was created using what is termed a "pot holder" loom. Although tedious, this method allows careful bending of the wires at the edges and results in undamaged cells. The wire density is quite close to that of the woven fabric: 32 cells per 6 inch width compared to 38 cells per 6 inch width of the woven fabric.

Measurements of this hand-made sample showed that a 1 ft^2 fabric could produce 330 mA of current at 1.2 V. Over a 4 hour charge time a 2,000 mAhr capacity AA nickel metal hydride battery would receive approximately 1,300 mAhr of energy. This is well over 50% recharge and within the contract requirements. We fully expect that a properly woven fabric would meet this performance level.

For additional power calculations, it may be important to know the fabric weight per unit area. Using samples of the OPV wire woven fabric we measured 0.51 kg/m^2.

Task 10 – Supercapacitor Ribbon and Thermal Scavenging Wires

We were prepared to incorporate these advanced concepts into the PV fabric, but the technology which was being developed under a separate Army contract was not yet ready to be demonstrated.

Detailed Description of Results - Tasks 1 – 7

When we started work on the current organic photovoltaic (OPV) fiber project, we were building on the results of an earlier Konarka Technologies, Inc. contract that was completed in 2009. The state of the research at the time left us with severe limitations for weaving large area PV cloth. The fill factor, which is a measure of how close the system being evaluated is to ideal, dropped off with the length of test sample so that with a 25-cm-length test sample, the fill factor was down to 25%. This was due to the low conductivity (high resistivity) of both the primary and secondary electrodes. We also had difficulty preparing finished fiber continuously in runs longer than a few hundred to five hundred feet due to severe twisting of the secondary electrode. The coating line is shown schematically as Figure 1.

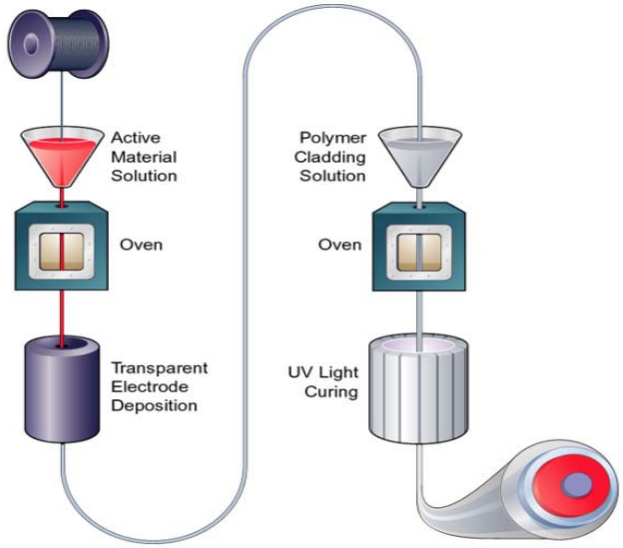

Figure 1. The coating line.

In addition, the efficiency of the primary electrode was not what it should have been, even for short test samples. The early work was all based upon a single semi-conductor, (P3HT - a commercially available polymeric thiophene) which was not thoroughly optimized for a stainless steel wire substrate. There are now many more choices of conductive HILs, e.g., hole injecting layer and polymers, for coating the primary electrode structure as well. The encapsulant used for the original project was formulated for dye-cell wire and was not easy to work with, nor was it particularly stable. There was not much success in designing methods and equipment to automate woven wire connections either. As we worked at solving these issues, other limitations

were revealed, including the need to have both electrodes composed of similar materials to allow for automated welding.

With all of these issues, it would be impossible to produce wire with the required consistent efficiency over long enough runs to allow weaving of 1-foot-wide cloth. We therefore needed to make improvements to all of the components and processes of the OPV wire production through systematic experimentation. This included:

1) Utilizing more efficient semi-conductors and optimization of the coating and annealing processes specifically for coating on stainless steel wire;

2) Changing from polished stainless steel to silver-cored steel for the primary, and later, for the secondary electrode substrate;

3) Modifying the Tetra-n-Butyl Titanate (TnBT) concentration, coating speed, and sintering temperature changes to primary electrode substrate wire;

4) Changing to a more conductive secondary electrode wire;

5) Using a copper cored silver wire as secondary electrode initially;

6) Changing from silver epoxy formulation to nano-silver ink for preparation of secondary electrode coated over silver cored stainless steel;

7) Using annealed silver-cored stainless steel for a more flexible secondary electrode for longer continuous, finished PV wire capability;

8) Using new conductive HIL materials and formulations;

9) Changing to more efficient semi-conductors and optimization of the coating and annealing processes.

Utilization of higher performance materials and process optimization

Optimization of P3HT/$PC_{60}BM$ Process

Before investigating new active polymers for PV wires, we optimized the coating and processing conditions for P3HT. In our original investigation we didn't spend a lot of time

optimizing the coating and processing conditions specifically for P3HT on stainless steel wire and felt that it was possible to significantly improve the efficiency of this system. Originally, we opted to use similar conditions of coating and processing previously optimized for preparing Konarka's "flat" modules. We found that in this original work, the P3HT polymer was coated too thick and was annealed using conditions that were too harsh. The thickness of the coated layer is controlled by the coating speed, the semi-conductor concentration, and coating fluid temperature. The final polymer morphology, and thus the efficiency, is influenced by the drying and curing rates. Therefore, with our coating and drying equipment, the coating speed and drying zone temperature were also important, as was choice of solvent and its evaporation rate.

We ran a set of experiments with 6.5% P3HT/$PC_{60}BM$ (a commonly used fullerene derivative) in which we varied coating speed: 10, 20, 35, and 50 ft/min, 50 ft/min being our control at the time (Figure 2). We also varied annealing temperature: 110, 120, or 130 °C. The HBL (hole blocking layer) and HIL were the same for all experiments. For all of these results the substrate was 4 mil stainless steel wire treated with TnBT at 525 °C, 10 ft/min. Relative humidity was controlled between 35 and 40%.

The efficiency was measured by taping the primary electrode coating to a glass slide previously coated with a silver epoxy coating. The ends of the slide were previously covered with an insulating layer of tape adjusting the active length to 5 cm. The tape used to adhere the primary electrode to the slide was Staples invisible tape; Scotch® brand tape somehow destroys the PV properties of the primary electrode coatings and cannot be used for this experiment. The fill factor reached an average of as much as 52.6% where we were previously looking at averages in the low 40s.

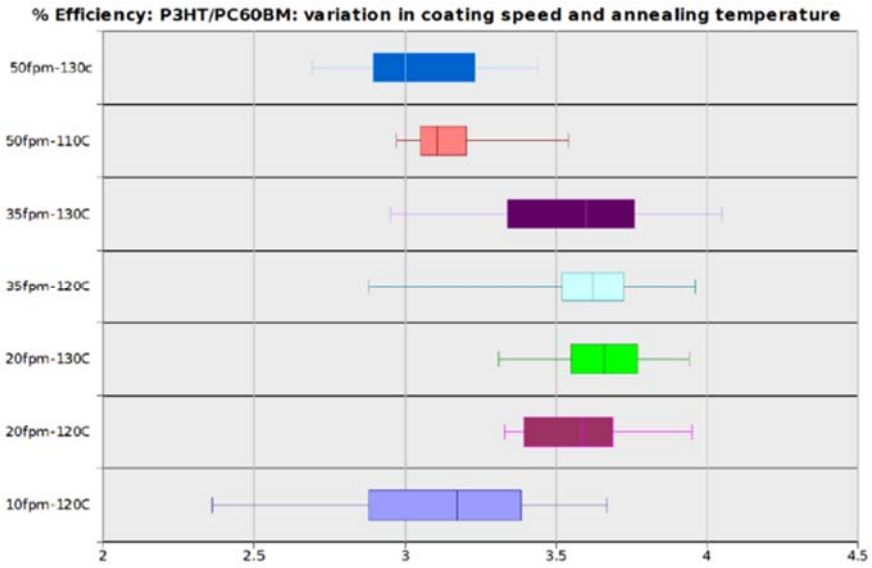

Figure 2. Efficiency box plot for P3HT/$PC_{60}BM$: variation in coating speed and annealing temperature.

In this set of experiments our highest average efficiency, fill factor, and P_{max} (maximum power point) were achieved with a 20 ft/min coating speed and 130 °C annealing for 5 min. The highest coating speed, 50 ft/min, yielded the highest current density. The lowest coating speed, 10 ft/min, yielded the highest average V_{oc} (open circuit voltage). Any variation of the concentration of the semi-conductor fluid would result in a different optimum coating speed. We kept this in mind moving on to more efficient semi-conductor polymers.

We also discovered that varying the solvent used to dissolve the semi-conductor(s) had a significant effect on the test results. We ran sets of experiments in which we replaced our control solvent for P3HT/$PC_{60}BM$ solution with the higher boiling solvent o-dichlorobenzene (o-DCB - boiling point of 180.5 °C compared to 144.4 °C). We found that the current density increased while to a lesser extent the fill factor decreased with an overall increase in efficiency. Some adjustment to the fluid concentration was made during optimization of the coating process for the o-DCB (ortho-dichlorobenzene) semi-conductor fluid further improving the results. The increase in IV (current-voltage) properties is due to morphological changes in the semi-conductor facilitated by the slower drying. See the data in Table 1 for averages of 10 measurements. There was as much as a 17% increase in efficiency with these changes. These results were transferable for use with other semi-conductors.

Table 1. Improvements with switch from o-xylene to o-DCB semi-conductor solvent.

Sample ID	Voc (V)	Jsc (mA/cm^2)	V_{max} (V)	I_{max} (mA)	J_{max} (mA/cm^2)	Efficiency (%)	Fill Factor (%)	R_{ser}*A ($\Omega \cdot cm^2$)
o-xylene control	0.6	13.3	0.46	0.52	10.44	4.77	60.07	5.51
o-DCB 6.5% sol'n	0.59	16.53	0.41	0.64	12.78	5.29	54.4	7.89
Change w o-DCB	-1.37%	19.20%	-8.59%	17.08%	17.13%	7.03%	-9.02%	49.93%
o-DCB w/6% sol'n	0.58	17.57	0.41	0.68	13.62	5.60	54.7	7.92
Change w o-DCB	-2.56%	32.14%	-10.03%	30.43%	30.43%	17.31%	-8.83%	43.60%

Several potentially better active polymers and combinations of active polymers were tested and a few of them yielded better efficiency than P3HT alone. Besides yielding better overall efficiency, we looked for polymers that would result in a higher fill factor that would drop off with increased length of wire gradually rather than precipitously. We also wanted robust materials that yielded consistency of the coated wire results from the beginning of a 1700-ft coating run to the end of the run.

Si-ZZ50/KP179 Semi-conductor Combination

We experimented with combinations of semi-conductors that worked well in experiments for Konarka "flat" cells. KP179 and KP184 are proprietary polymers from Merck. Si-ZZ50 is shown as Structure 1.

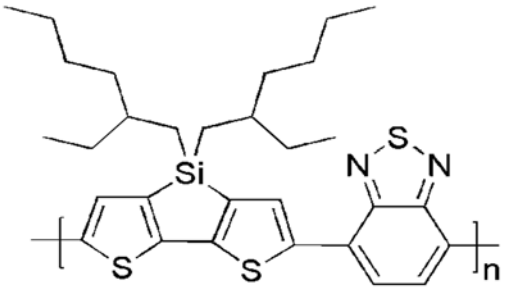

Structure 1. Si-ZZ50

Both KP179 and KP184 when combined with Si-ZZ50 yielded improved IV performance compared to P3HT alone. With the SiZZ50/KP179 combination, we saw for the first time average efficiency values of greater than 6% as measured using the silver epoxy coated glass slide measurement described above. A primary wire consisting of SiZZ50/KP179 coated over silver-cored stainless steel wire was mated with a copper-cored silver wire and encapsulated with Perma-Bond UV683. This yielded efficiency values of as high as 5% for 10-cm segments of finished wire. From this finished wire we were able to prepare a working sample consisting of 13 2-ft long segments connected in series with silver epoxy and adhered to a piece of beige canvas. The efficiency of this "woven" piece of PV cloth was 5.52% as measured at one sun in the Oriel solar simulator (Figure 3).

Although this semi-conductor combination yielded the best performance we had seen, we were not able obtain consistent results with the coated primary electrode. We got inconsistent run to run results with the primary coating and, the longer the coating run, the more the performance dropped off.

Other materials that yielded efficiency results similar to the SiZZ50-KP179 combination included: KP306 alone, SiZZ50 with KP184, and P3HT with ZZ83. Of these, only the P3HT-ZZ83 combination yielded consistent results both with run to repeatability and throughout a 1600 to 1700-ft coating run.

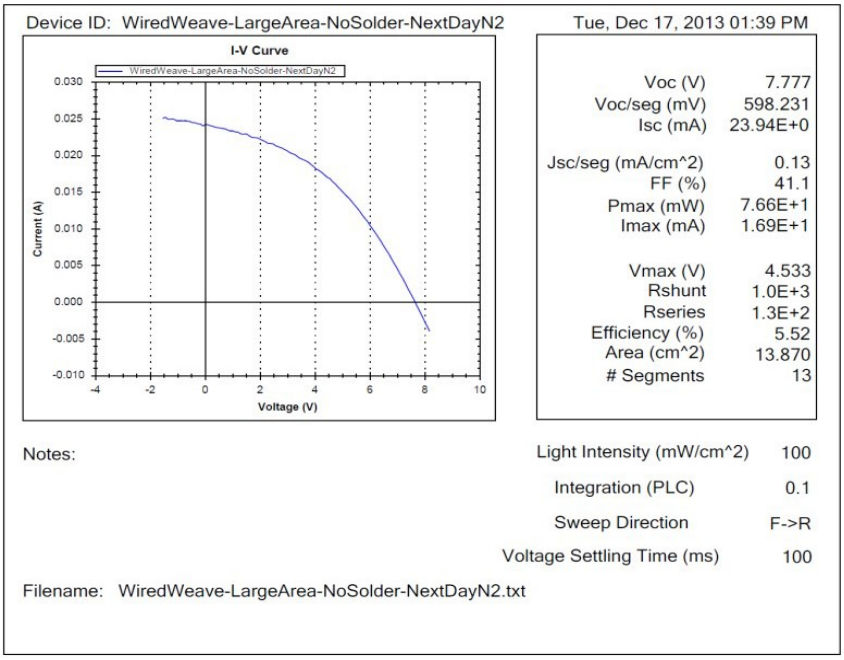

Figure 3. IV curve for the 13 segment sample.

P3HT/ZZ83/PC70BM (3:1:1 in o-DCB)

By adding a second semi-conductor polymer, ZZ83, to our P3HT fluid, we found that we could reach much higher current density than with P3HT alone. Also, we had to coat with a significantly lower fluid concentration than we found to be optimum for P3HT/PCBM fluids. The ratio of materials added in this fluid formulation are the same as those used in Konarka's flat OPV controls. We used o-DCB as the solvent where the Konarka fluid used a combination of o-xylene and tetralin.

Figure 4 shows plots of IV parameters versus fluid concentration for coatings prepared with a 25 ft/min wire coating speed. These measurements were all done with wire samples taped to silver epoxy coated glass slides. The current density, Jsc, reached as high as18.5 mA/cm^2 on average. Although this is short of the >21 mA/cm^2 reached with SiZZ50/KP179 earlier, the higher fill factor with P3HT/ZZ83 leads to nearly equivalent average efficiency.

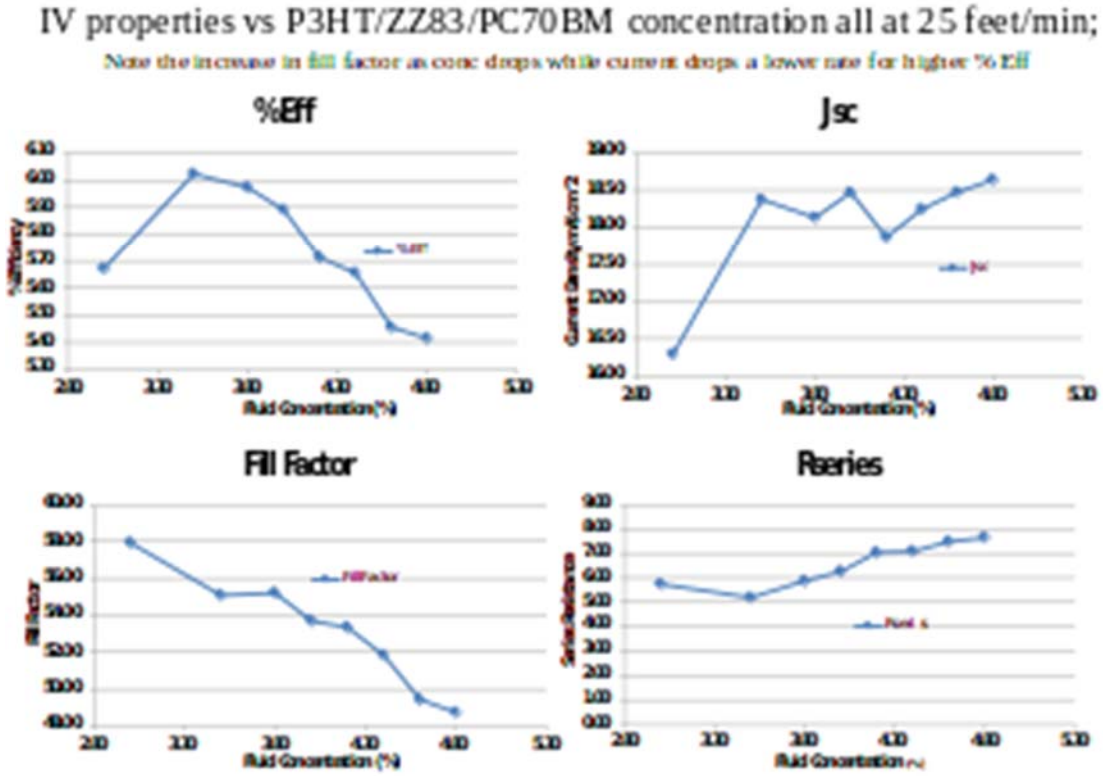

Figure 4. IV properties vs. fluid concentration for P3HT/ZZ83 blend in o-DCB.

We found the reproducibility for the P3HT/ZZ83 combination, both run to run and within run, to be much better than that of SiZZ50/KP179. For this reason we decided to use P3HT/ZZ83 coated on silver-cored stainless steel for our primary electrode in scaling up OPV wire runs for large area weaving. To this end, we coated several runs of 1500 to 1700 ft in length and produced final OPV wire using either of two secondary electrodes: a nano-silver ink coated silver-cored stainless steel wire or a copper-cored silver wire.

The average efficiency for each of the ~15 spools of finished fiber was between 3.3 and 3.8% for the nano-silver coated secondary wire as measured in 50-cm segments against the flat black surface of the solar simulator/tester. The average efficiency is a little higher with the copper-cored silver secondary electrode. When measured against a piece of off-white canvas, the efficiency jumped to greater than 7.7%. For OPV wire made with the copper-cored silver secondary electrode the increase is even more substantial, jumping to greater than 8.5% efficiency. See the example curves below in Figures 5 and 6. The woven fiber with a white cotton thread should yield readings closer to those made against the canvas.

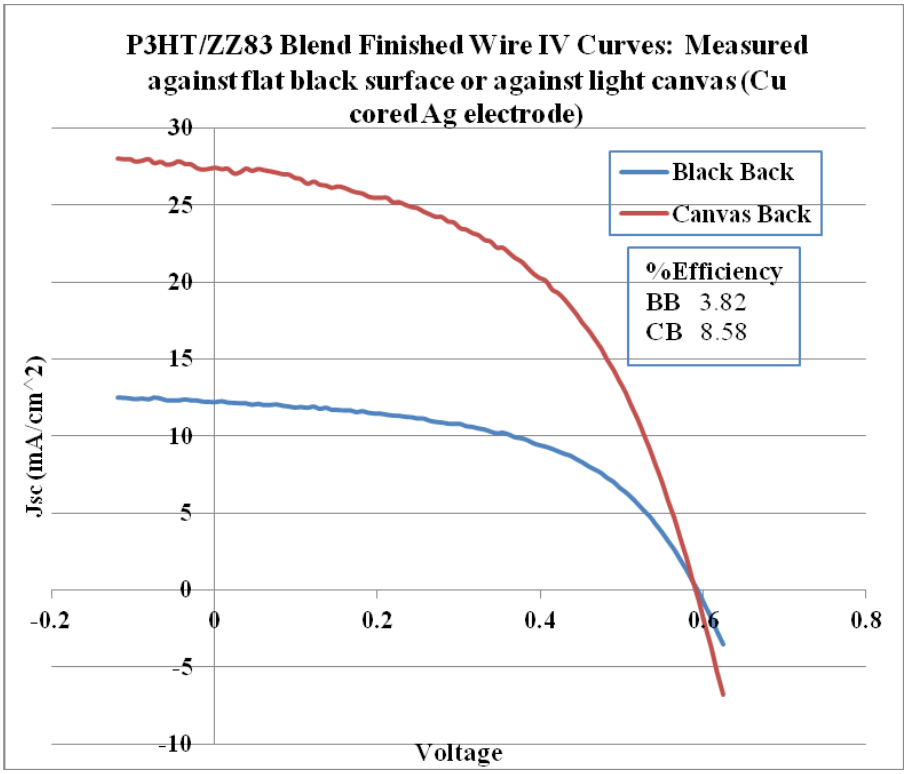

Figure 5. Black metal vs. light canvas as background for measurements of IV properties of OPV wire w/nano-silver secondary electrode.

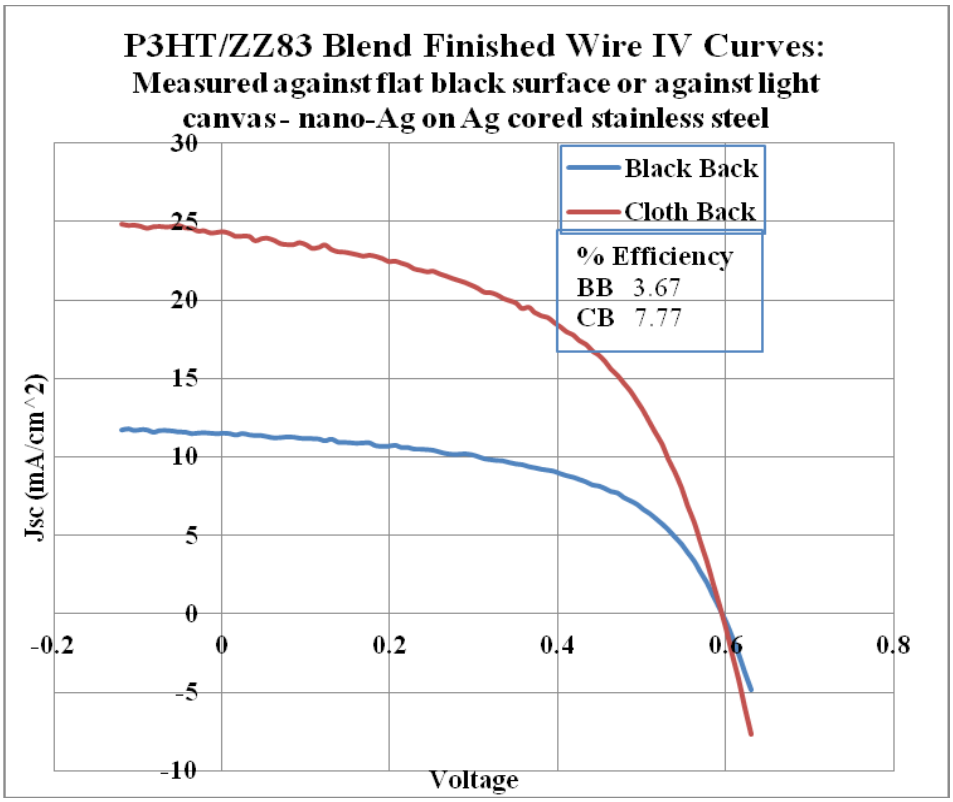

Figure 6. Black metal vs. light canvas as background for measurements of IV properties of OPV wire w/copper-cored silver secondary electrode.

We prepared over 30,000 ft of finished wire. All of it was made with P3HT/ZZ83 blend coated silver-cored stainless steel primary electrode. For the secondary electrode we used nano-silver ink coated over annealed silver-cored stainless steel for the majority of the finished wire. For the remainder, we used copper-cored silver wire from Ulbrich Stainless Steels and Special Metals, Inc. in keeping with our aim for flexible OPV wire for easier weaving with much less twisting in the finished fabric.

Silver-cored primary and secondary electrodes and TnBT Process Optimization

In order to produce an efficient woven fabric we needed to improve the conductivity of both our primary and secondary electrode wires. In our earlier experiments and for the first few months of this project, we used diamond-drawn 316 stainless steel wire. We needed a more

conductive starting wire and found that our supplier for the 316 stainless steel wire now had the capability to supply the same diamond-drawn 316 stainless steel wire with a silver core.

In order to conserve our inventory of silver-cored stainless steel wire, we did a lot of our semi-conductor optimization experiments with 316 stainless steel wire manufactured by Fort Wayne Metals. When we later did some coating experiments with silver-cored 316 stainless steel wire, also manufactured by Fort Wayne Metals, we unexpectedly saw poorer initial IV properties than expected. We suspected that the silver-cored stainless steel wire may have been annealed at too high a temperature since silver is a much better conductor of heat (> 25x - see Table 2).

To test this hypothesis, we did an experimental temperature series for the TnBT annealing process. We coated 1% TnBT (tetra n-butoxytitanate) at 10 ft/min and varied the furnace temperature incrementally from 400 °C to 480 °C. We then coated the TnBT treated wire samples with a control OPV structure, hole blocker/P3HT-ZZ83 semiconductor/HIL. We annealed pieces of each OPV coating for 3 m at 120 °C before measuring IV properties as taped to silver epoxy coated glass slides. The primary wire testing results with the annealing temperature range of 400 to 440 °C is much better than that with higher TnBT annealing temperature (Figure 7).

Table 2. Resistive properties of wires used in PV wire processes.

Sample	**Diameter (in)**	**Sample Length (in)**	**Resistivity (Ω)**
Fort Wayne, SS, Lot # C-40663 5/14/07	0.004	12	30
Fort Wayne, Alloy (#3 or #4)	0.004	12	40
Fort Wayne, 316 LVM, 41520, Annealed	0.004	12	31
Fort Wayne, 316 LVM, 41520, "As Drawn"	0.004	12	32
Fort Wayne, 316L-DFT-30%Ag	0.004	12	2.1
Fort Wayne, 316L-DFT-30%Ag	0.004	12	2.3
Fort Wayne, 316L-DFT-30%Ag-coated with UT Dots Nanosilver	0.004	12	2.3
California Fine Wire, SS	0.002	12	138
Ulbrich, Silver Plated Copper	0.0034	12	0.7
Nanocomp, Carbon Fiber, 100330, Lot #10005		12	198
Nanocomp, Carbon Fiber, 100080, Lot #643201		12	447

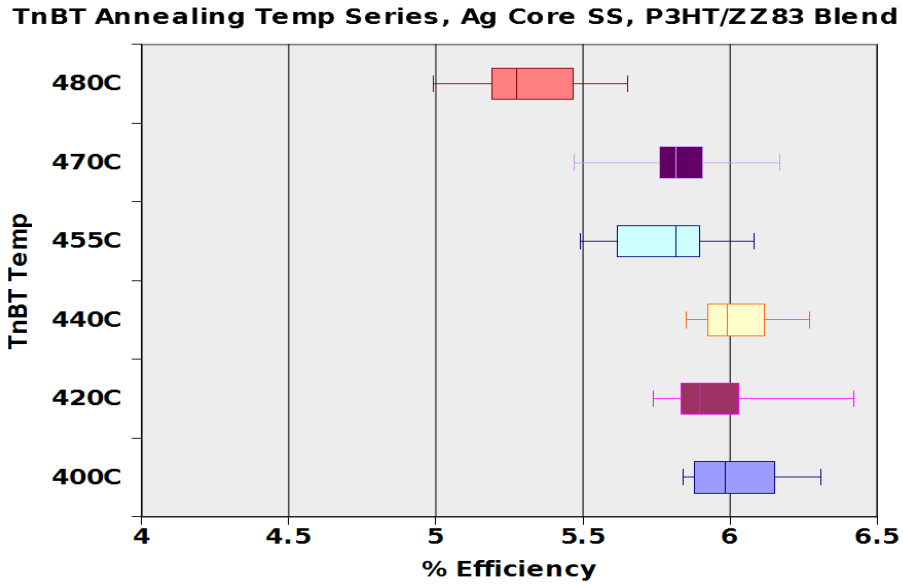

Figure 7. Efficiency versus TnBT annealing temperature for P3HT/ZZ83 blend primary.

In the earlier PV wire project, we coated a 2-mil 316 stainless steel wire with a heat-curable silver epoxy. Since the viscosity of this silver epoxy formulation increased with time, so did the thickness of the coated layer. This limited the length of secondary electrode to less than about 1000 ft but usually less than or equal to about 500 ft. The resulting irregular coating of the silver epoxy on the wire led to plugging of the polymer extrusion applicator during the finishing process, further decreasing the average continuous length of finished wire. We managed to find a much better alternative with an off the shelf copper cored silver wire available from Ulbrich Metals.

Although we had very good efficiency results using the copper-cored silver secondary electrode from Ulbrich, we needed to find a secondary electrode with similar melt properties to the primary, silver-cored, stainless steel electrode. This was necessary for our automated welding process. To this end, we started exploring the same silver-cored stainless steel used for the primary wire only without TnBT treatment and with an added layer of silver over the stainless steel. We had the option of having the silver-cored stainless steel wire plated with silver by Fort Wayne Metals or coating a conductive silver layer over the silver cored stainless steel wire ourselves.

We obtained samples of the silver-plated wire from Fort Wayne Metals and this worked very well in initial testing. The silver-plated wire required such a long lead time for ordering, we decided to further explore silver coating options. We tried coating silver inks over the silver-cored stainless steel wire and found that a nano-silver ink supplied by UT Dots, Inc. worked quite well. We initially had some varying results with these two methods and they did not yield results as good as those achieved with copper cored silver secondary electrode. Nevertheless, we still saw fill factor readings averaging up to 60% or more for a 1-m-long wire for these silver-plated or coated silver-cored stainless steel secondary electrodes (Figure 8).

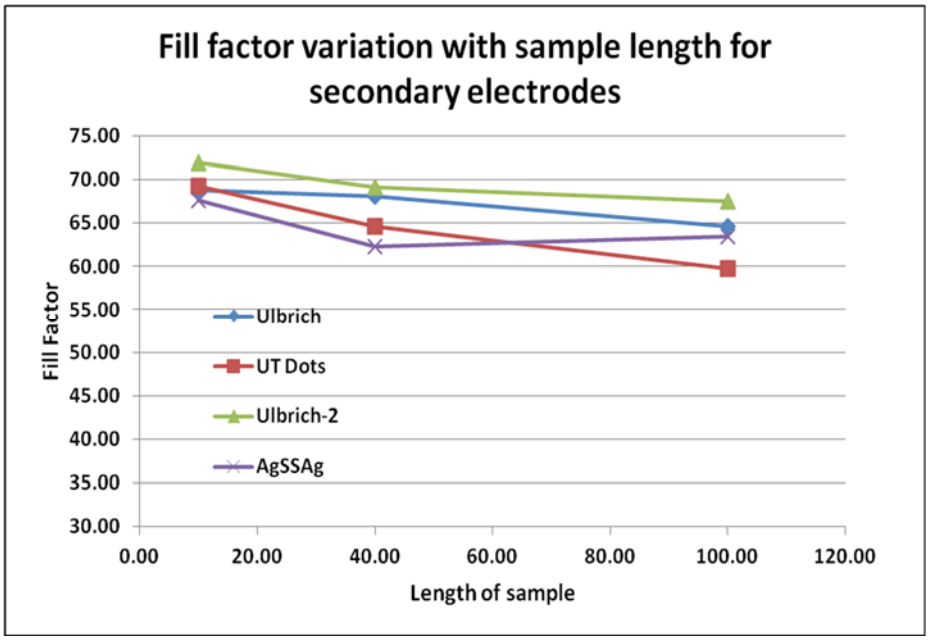

Figure 8. Change in fill factor with increased length of OPV wires with different secondary electrodes.

When we prepared finished PV wire using either of the electrodes prepared with the silver-cored stainless steel, we found that the longer the run, the poorer the results. We could see that with the as-drawn silver-cored stainless steel wire there was a tension build-up as the wire finishing run progressed. We did not have this problem with copper-cored silver wire because it is much more flexible. We sensed that this issue would therefore be resolved if we had the silver-cored stainless steel wire annealed at Fort Wayne Metals.

Tension Build-up in the Stainless Steel Electrodes

We believed that the major reason for the tension build-up in the secondary electrode began with the stiffness of the as-drawn (non-annealed) silver-plated or nano-silver coated silver-cored stainless steel wire. When wound on our feed spools, these secondary electrodes had a memory of the spool shape that built up over time. The wire formed stiff coils that were hard to wind around the primary electrode wire. We didn't see nearly as much of this effect with copper-cored silver secondary wire that is much softer and more malleable. We ordered annealed silver-cored stainless steel wire expecting it to be much softer and less prone to coiling memory. When this annealed silver-cored stainless steel wire was coated with UT Dots, Inc. nano-silver ink it did, in fact, work quite well.

Pieces of the finished wire prepared with UT Dots, Inc. nano-silver secondary electrode from the beginning and the end of a spool were not significantly different. Sample curves are shown in Figure 9 for an example from a 1620-ft continuous run.

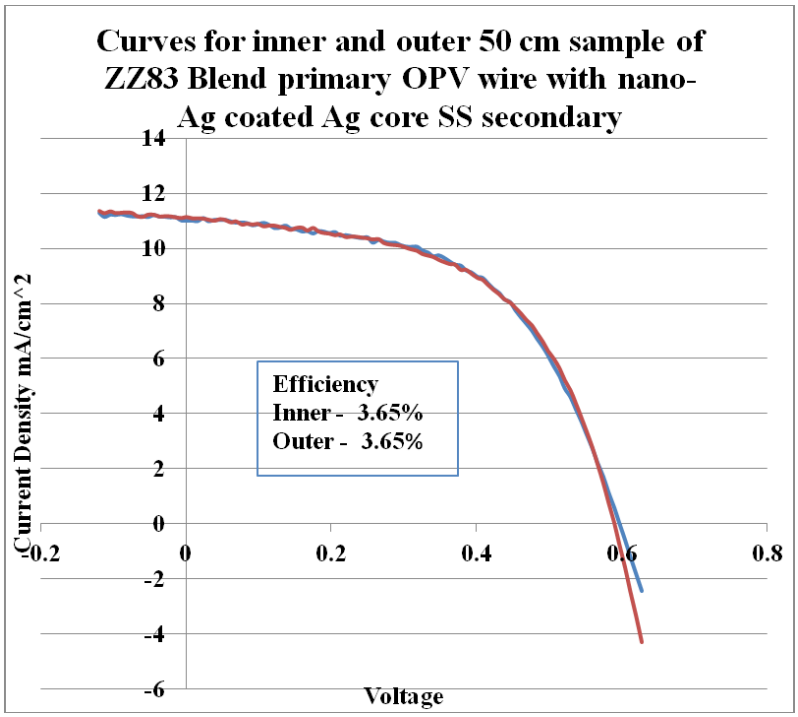

Figure 9. Inner and outer sections of a 1620 ft encapsulated wire comprising P3HT/ZZ83 blend.

High Conductivity HILs

When optimizing the primary electrode coating materials and process, the HIL layer cannot be ignored. In the previous project, we found that Clevios PHCV 4 (a commercially available HIL polymer formulation) worked well but there are many new highly conductive HILs available now. We ordered several of these new HILs and tested them with our primary electrode coatings.

The best of the new conductive HILs that we tested are Clevios HTL Solar and Clevios PH 1000, both manufactured by Heraeus. Both of these formulations yielded better efficiency than Clevios P HCV4, our previous control. This is illustrated in Figure 10. A big improvement in the efficiency is seen, and we found that the PH 1000 HIL yields fairly stable results while HTL Solar showed a loss of > 8% after only 4 days of storage under nitrogen/vacuum compared to no loss for PH 1000. Another conductive HIL, Clevios FHC Solar, yielded even better initial

testing results but had no stability at all due to the inclusion of dimethylsulfoxide, a powerful solvent, in its formulation.

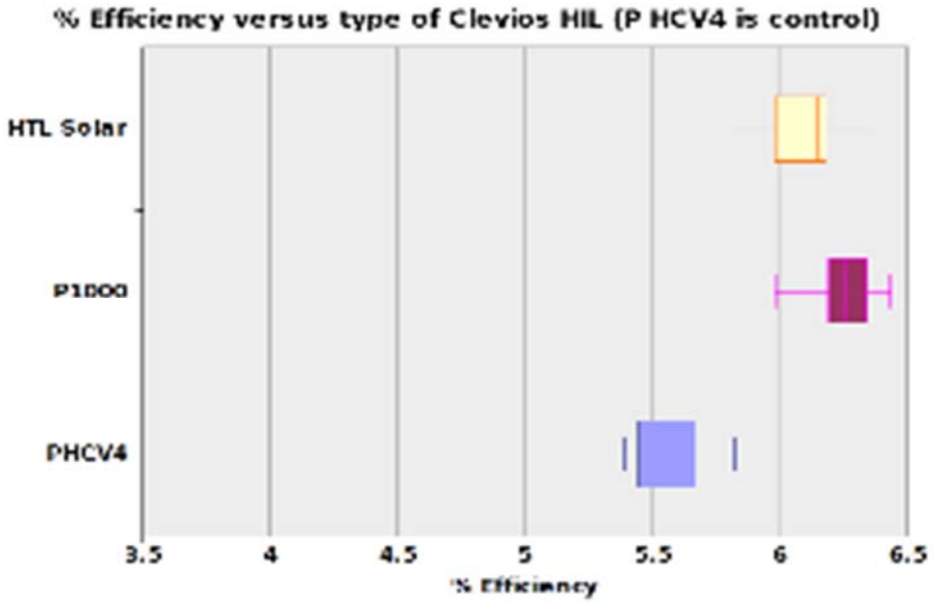

Figure 10. Efficiency for three conductive HILs with P3HT/ZZ83/PC70BM blend semi-conductor.

High Refractive Index Cladding Formulations

We have seen improvements in light utilization when we incorporate appropriate levels of light scattering particles in the polymer cladding. We experimented first with TiO_2 particles added to the polymer as a means of increasing internal reflection of light in the polymer encapsulant. With one type of TiO_2 nano-particles we saw as much as a 15% improvement in the efficiency of our OPV wire. This improvement turned out to be relatively short lived as the TiO_2-containing encapsulant yielded fairly large losses in IV parameters over a relatively short time and after 60 days had lost > 20% of the original efficiency compared to about 10% loss for the control. This is likely due to some residual “poison” component of the particle production process. We experimented with other types of TiO_2 particles that are less likely to have the same stability issues and saw similar initial results.

As an alternative to TiO_2 particles we did several experiments with Perkalite F100S (Akzo Noble) clay particles in our control Permabond UV683 (a commercially available acrylate polymer) cladding. We previously used encapsulant formulations that included Perkalite in

Konarka flat cells and saw no negative stability issues. We tested as high as 30 weight % Perkalite in Permabond UV683, but we found that lesser amounts in the clay resulted in better coating uniformity over the wires and also led to > 10% efficiency improvement in the finished OPV wire (Figure 11). The improvement is primarily due to increased current density. Due to the plate-like shape of the clay particles we hope to see an improvement in stability as well due to their creation of a more tortuous path for moisture and oxygen through the polymer coating.

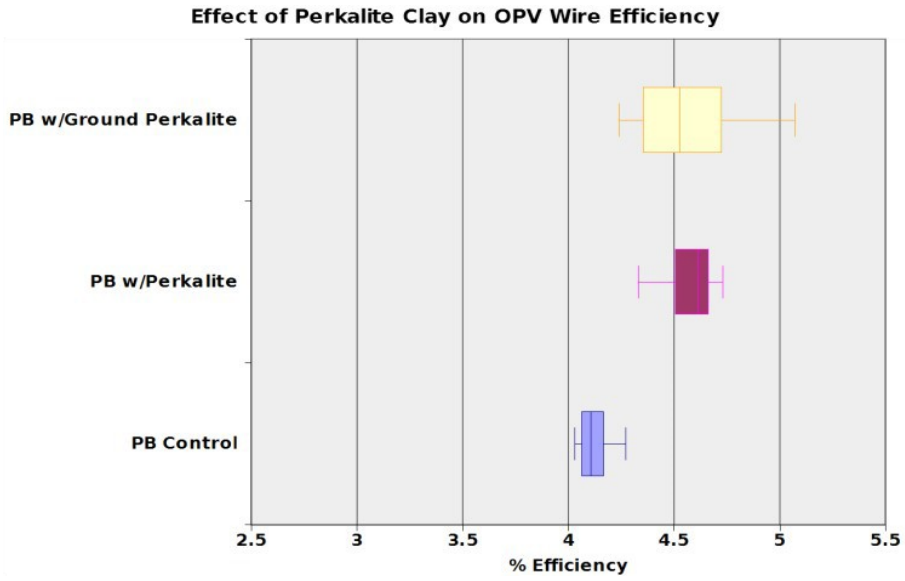

Figure 11. Improvement in OPV wire efficiency with Perkalite clay particle incorporation in encapsulant polymer formulation.

This improvement in efficiency with the addition of Perkalite does not adversely affect the stability of finished wire. In fact, in an application where a refractive index-increasing additive adversely affected stability by itself it had no negative effect in the presence of the Perkalite clay. This is illustrated in the box plots of Figure 12.

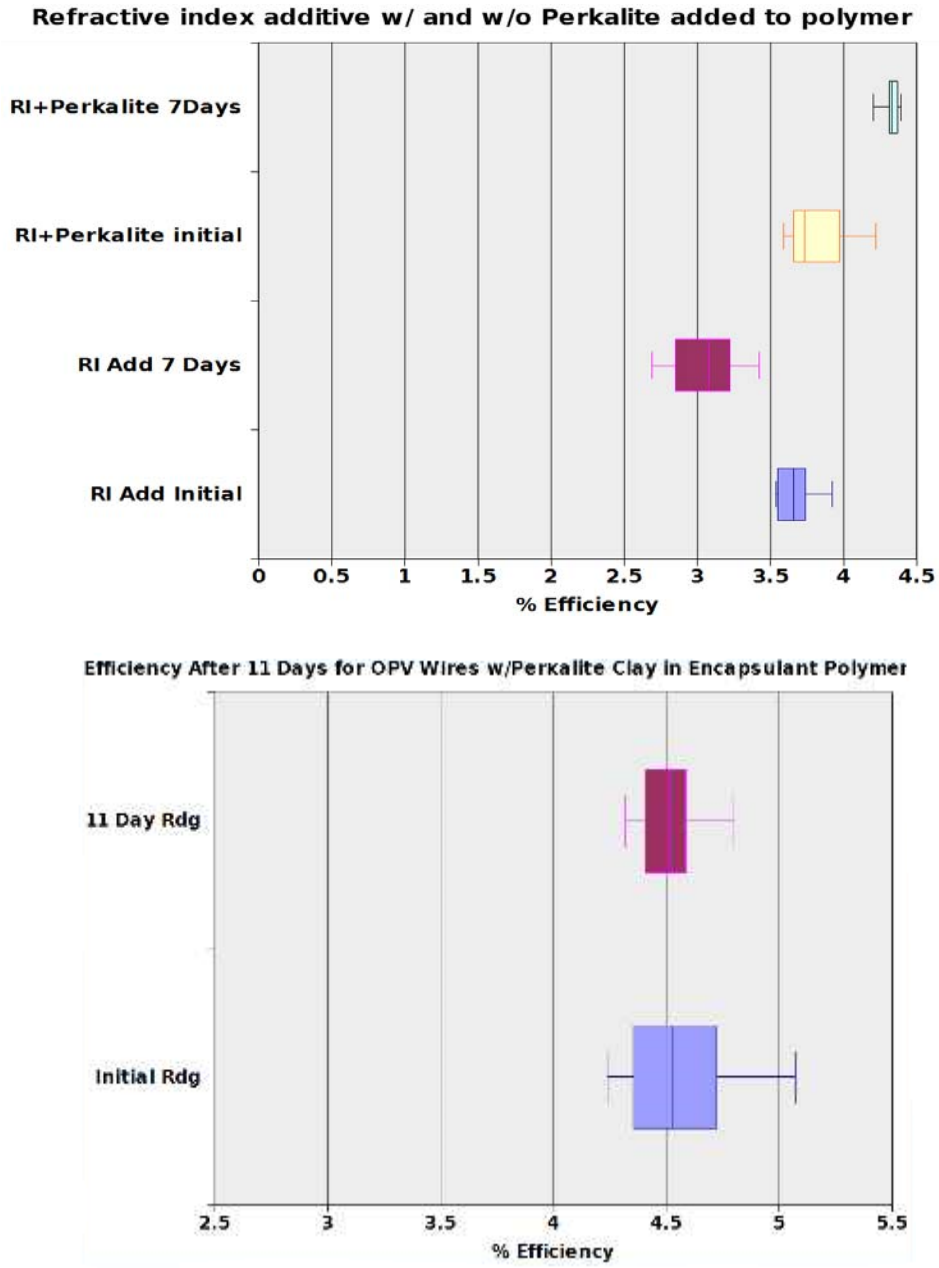

Figure 12. Enhancement of efficiency stability of index-enhanced encapsulants with Perkalite (top); efficiency stability with Perkalite alone in encapsulant (bottom).

Production of OPV wire for weaving

As mentioned in the May 2014 report, nano-silver ink coated on annealed silver-cored stainless steel resulted in a secondary electrode that did not significantly build up tension during our final assembly process. We were able to produce PV wire continuously up to greater than 1700 ft in length with no secondary wire breakage. Pieces of the wire from both the beginning

and end of the finished spool were not significantly different. Refer to Figure 8 for examples of the performance of a 1620-ft continuous run.

Up to three runs worth of wire, or about 4800 to 4900 ft, were combined by rewinding. Prior to use in the weaving trials, the spools of wire were stored under vacuum with a nitrogen back flush. This wire was used for the large sections of woven cloth generated by UMD.

Plasmon Enhanced PVs

The Clemson group produced samples of plasmonic nanoparticles that, in principle, could have resulted in PV wires that showed an enhanced PV efficiency due to an antenna effect. In fact, a reduction in efficiency was seen. In a system of this complexity, many types of interactions are possible and possibly here the optical absorption of the plasmonic coatings outweighed any antenna effect. Clumping of the particles and unfavorable interactions between the organic components of the PV system and the particle suspension should be considered in any future pursuit in this area.

Clemson University is pursuing this study on a simpler inorganic flat PV system where it may be easier to demonstrate the antenna enhancement before returning to organic systems.

Task 8 - Automated Welding

Wire Interconnect Process – General Description

The system for connecting the primary and secondary PV wires to a pair of bus wires involves a welding unit to bond the wires and provide a good mechanical and electrical connection. As shown below in Figure 13, the primary and secondary PV wires protrude from the edge of the cloth fabric, and the bus wires run parallel to the fabric edge along its length. In the simplest arrangement, all the primary wires are welded to one of the bus wires, and all the secondary wires are welded to the other bus wire. This provides a parallel wiring scheme where one bus is positive electrical polarity relative to the other bus wire, and the voltage is that of a single PV wire, typically about 0.6 V. Alternate connection arrangements can be implemented where the PV wires are connected in different series and parallel combinations to obtain higher voltages.

In order to make electrical connections between PV wires, the cladding must first be completely removed. Hence, a major undertaking will center on automating the removal of the wire cladding. At the present time two methods have been demonstrated that effectively remove the cladding. The first is the commonly used thermo-mechanical wire stripping process using a set of metal jaws. When the jaws are completely closed on the end of a wire and drawn along the wire, the cladding is completely removed. The drawback to this approach is related to the high density of wires protruding from the edge of the fabric that must be stripped of cladding. In order to prevent damaging the wires themselves, every wire must be aligned with a hole, the diameter of which is equal to the diameter of the wire, in the edge of the closed jaws before stripping.

In the second approach, all of the wires protruding from the edge of a length of fabric are soaked in a solvent that swells and softens the cladding. A set of blade-like, rubber jaws are clamped on the ends of all of the wires whereupon the cladding is readily stripped from all of them simultaneously. The drawback to this approach is the use of volatile solvent and the length of soak time required (30 s at room temperature) to soften the cladding.

The welding setup has undergone several modifications as the work progressed. Key parts of the setup, including the Cognex vision system (a high definition camera and sensor) the X-Y moveable platform, the main controller (a programmable logic controller or PLC), and the welder are integrated and operating as designed. Refinements were made to optimize the

software and improve some mechanical operation. Using a Miyachi Unitex welder, the welding process, including welding voltage and dwell time, has been optimized. We have shown that the primary and secondary electrode wires can be identified and welded to the bus wires with 100% yield.

Referring to Figure 13, the PV fabric is placed on an X-Y moveable platform, and the PV wires are located across the two bus wires. Starting at one end of the fabric, the platform moves the cloth and precisely aligns the first PV electrode wire (either the preselected primary or the secondary) directly over the welding electrode. The Cognex vision system determines if this wire is the primary or secondary PV wire, and the main controller uses this information to determine whether to weld this wire to the bus. If it is determined that no weld is to be made, the X-Y table moves to the next electrode wire and the welder then welds this wire to the bus.

This sequence continues until all of the primary electrode wires are welded to one bus and all of the secondary wires are welded to the second bus. The fabric with the welded wires is then fully functional and, upon exposure to sunlight, is ready to power a device or charge a battery.

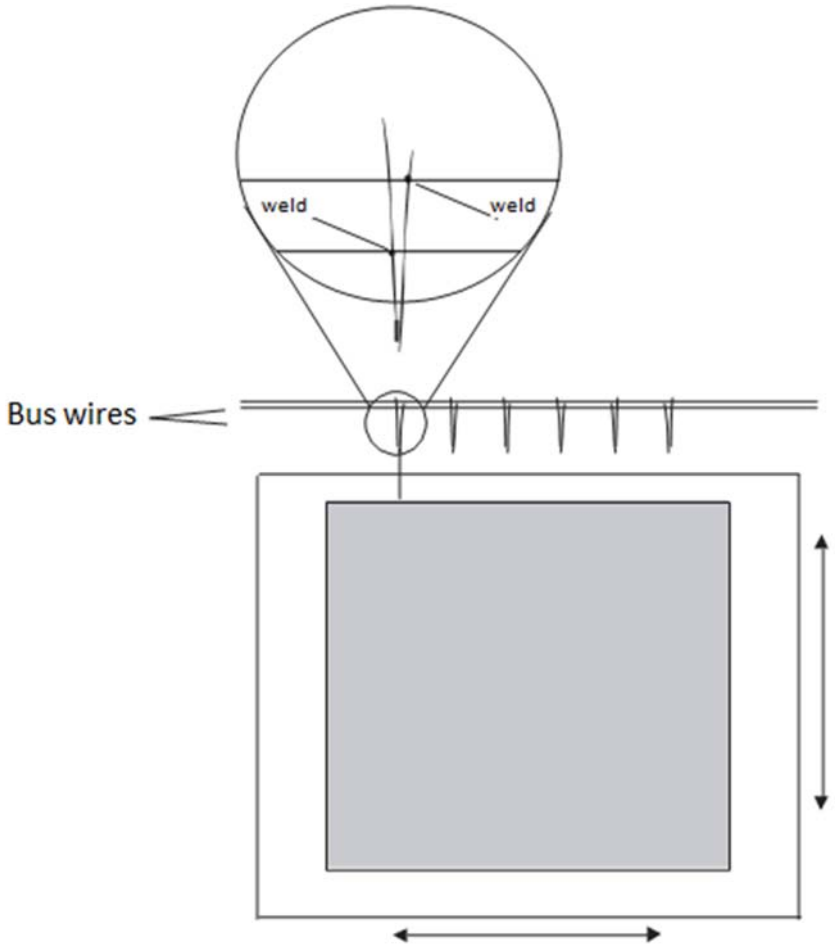

Figure 13. Schematic view (top) of the welder setup

Detailed Description of the Vision System and the Welding Operation

Any wire connection system must be able to distinguish between the primary and secondary OPV wires. A vision system is used to accomplish this task. The unit used for the wire connection portion of the program is manufactured by Cognex Corp. This vision system uses a digital camera focused on the lower welding head to detect when an OPV wire crosses into the field of view. The vision system is programmed to distinguish between primary and secondary OPV wires and send this information to the PLC unit. Three vision system software tools are used to accomplish this:

1) Filter_1 - This is a tool to convert all pixels in a defined region to either black or white. Pixels can have one of 256 shades of gray, and the conversion value is adjustable. The

purpose of this tool is to maximize the detection accuracy. A primary OPV wire is dark or black, while a secondary OPV wire is a shade of gray.

2) Find_Wire_Edge - This tool is set to locate an edge of the incoming wire and subsequently activate a related tool to count the number of dark pixels within a defined region. The Dark_Pixel_Counter tool is OFF until a wire edge is detected.
3) Dark_Pixel_Counter - This tool is activated when a wire edge is detected. It counts the number of dark pixels in a defined region to determine if the detected wire is a primary (dark appearance) or secondary (light appearance). Since Filter_1 has converted all pixels in the region to either black or white, the Dark_Pixel_Counter tool does not have to distinguish shades of gray. This makes the dark pixel count more precise. For this project, the proper dark pixel count was determined to be 85. A dark pixel count of less than 85 means the detected wire is a secondary OPV wire, while a dark pixel count equal to or greater than 85 signals a primary OPV wire. The size of the Dark_Pixel_Counter detection area can be adjusted to optimize the detection accuracy.

Figure 14 illustrates the operation of the vision system. As primary and secondary wires move across the lower welder electrode, the vision system optical tools (shown as green rectangles below) determine the type of wire and send the information to the PLC that operates the welding system. In the screen display below, the vision system correctly identified the primary OPV wire on top of the welder electrode. Note that the dark pixel count is 302, well above the 85 threshold and clearly identifying a dark or primary wire.

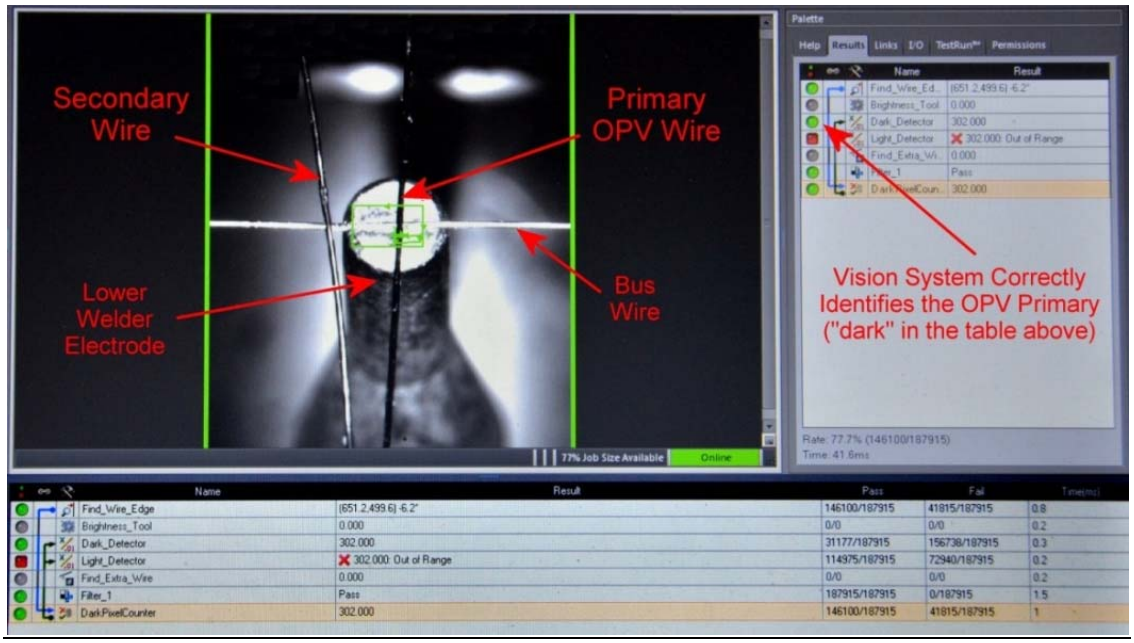

Figure 14. Vision system display identifying the Primary OPV wire (the “dark” wire)

Upon receiving this information from the vision system, the PLC determines whether to weld this wire or move on to the next one. Figure 15 shows the vision system display when a secondary or “light” wire is identified. Note that the dark pixel count is 18, well below the threshold of 85 and clearly a secondary or light shaded wire.

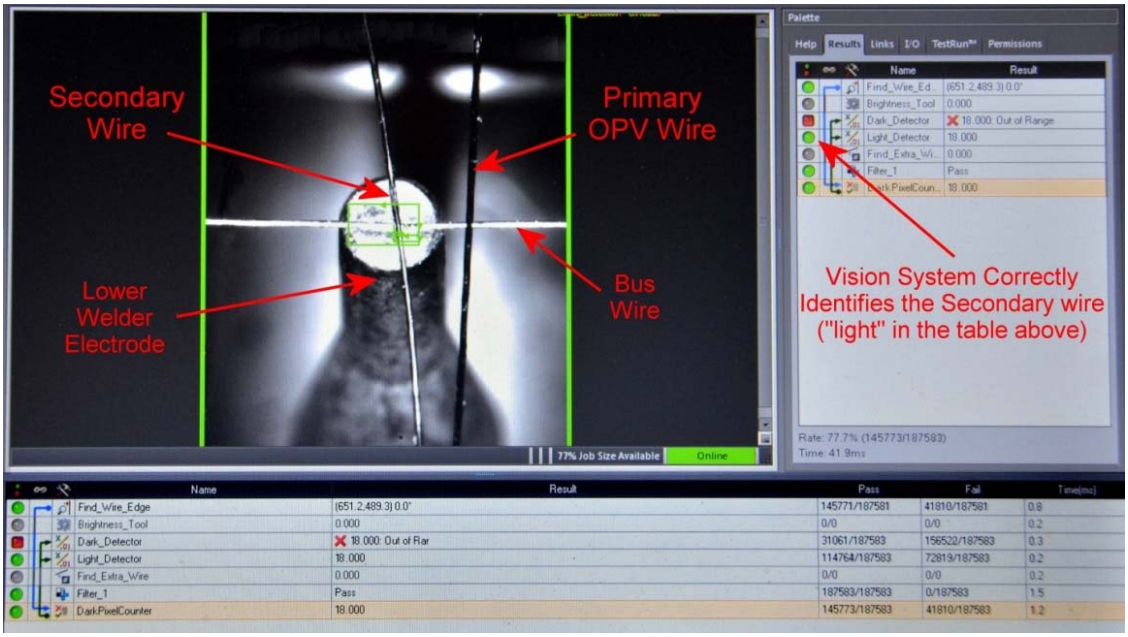

Figure 15. Vision system display, identifying the Secondary wire (the “light” wire)

Welder Equipment and Operation

The welder equipment and setup is shown in Figure 16. The wires to be welded are adjacent to the welder electrodes which are labeled in the figure. This area is brightly illuminated by an LED ring light attached to the end of the camera and just above the electrodes.

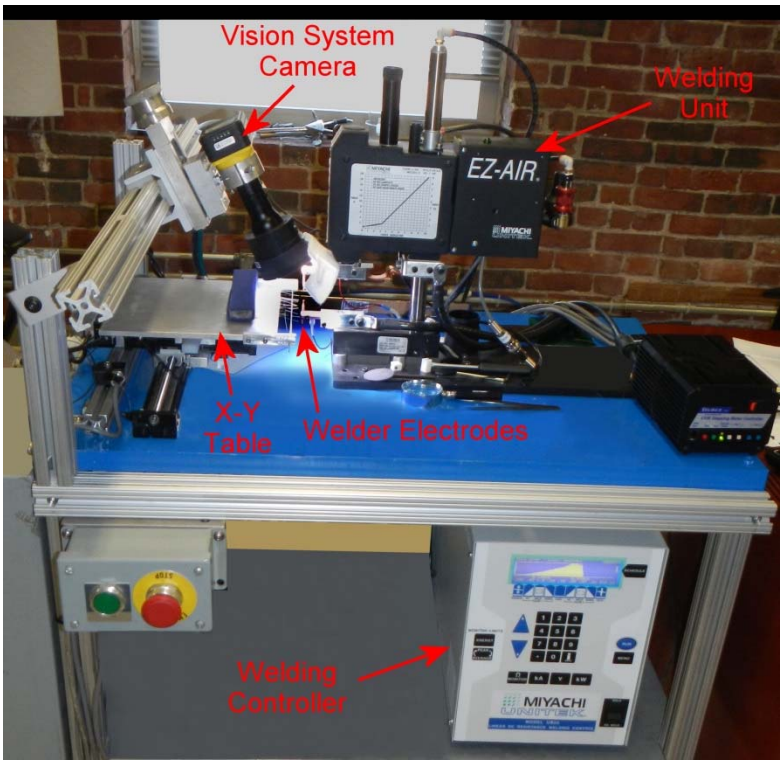

Figure 16. Welder setup, including vision system camera

A successful method to connect the OPV wires to bus wires was developed using a technology known as DC resistance welding. Resistance welding, also known as "spot welding", is a thermal-electric process in which heat is generated at the interface of the metal parts to be joined by passing an electrical current through them for a precisely controlled time under controlled pressure. In our setup, an OPV wire is laid across a bus wire and positioned between two copper electrodes of the welder. The compressed air-activated electrodes come together, sandwiching the crossed wires at a preset pressure, and a large DC current is passed through the contact point of the OPV/bus wires. Resistive heating at this contact point welds the wires together, forming both an electrical and a mechanical connection. Since the electrical resistance

between the copper electrodes and the OPV or bus wire is significantly less that that between the OPV and bus wires themselves, there is no melting at this interface with the copper.

It is critical that the DC current waveform be tailored for optimum weld properties. For example, oxides that are present on the wire surfaces must be broken down in order for the welding current to flow. In our process, this requires two separate weld pulses: first, a shorter pulse to break through the oxide layers; and a second, longer and larger pulse to actually weld the wires together. This is discussed in more detail below.

The equipment for the DC resistance welding was manufactured by Miyachi America Corp., which specializes in precision welding products. The specific model of the power unit is: UB25 Linear DC Resistance Welding Control. The front of the unit is shown below in Figure 17.

Figure 17. Front side of the Miyachi Welder. Note the waveform display screen at the top.

After much experimentation, the optimum DC pulse waveforms were identified. Figure 18 shows the preferred waveforms on the welder monitor. Note that there are two separate pulses, as described above.

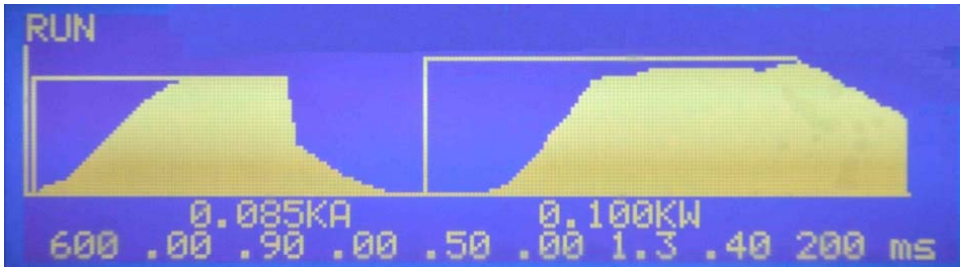

Figure 18. Welder waveforms after completing a successful weld

The waveforms shown were displayed after a successful weld operation. The Miyachi controller allows customization of the individual pulses. Below is a listing of the setup parameters that were used in this project.

- Squeeze time (the duration of electrode contact prior to the weld pulses): 600 ms
- Pulse 1 Setting: Current Mode - DC current limited to 100 Amperes, maximum
- Pulse 1 rise time: 0 ms (programmed to minimum time, actual risetime is determined by the resistance of the OPV wire/bus interface)
- Pulse 1 Duration: 0.90 ms
- Pulse 1 fall time: 0 ms (programmed to minimum time)
- Cool Time Between Pulses: 0.50 ms
- Pulse 2 Setting: Power Mode - power limited to 95 Watts, maximum
- Pulse 2 risetime: 0 ms
- Pulse 2 Duration: 1.3 ms
- Pulse 2 fall time: 40 ms
- Cooldown time: 200 ms (the time duration after the welding pulses that the electrodes remain in contact with the wires)

After a weld operation the individual electrical parameters can be displayed on the controller monitor.

Figure 19 indicates that the peak power for pulse 1 was 90 Watts and 96 Watts for pulse 2. The peak power for pulse 2 is just slightly above the programmed maximum setting of 95 Watts.

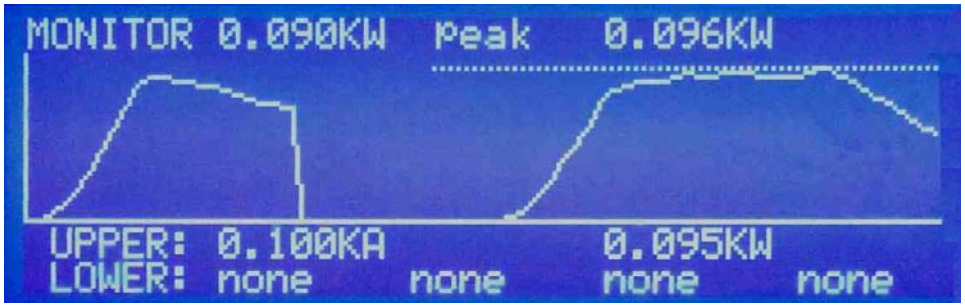

Figure 19. Welder pulses for a typical weld operation

Figure 20 indicates that the peak current for pulse 1 was 87 Amperes, less than the programmed maximum value of 100 Amperes. The peak current for pulse 2 is 121 Amperes - there is no current limit for pulse 2.

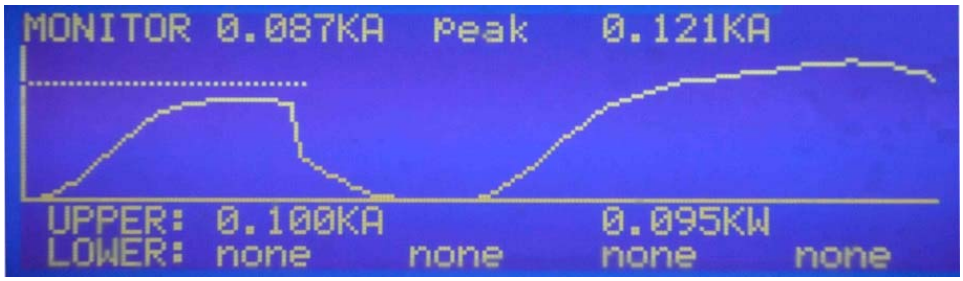

Figure 20. Welder current for a typical weld operation

Figure 21 shows the benefit of the 2-pulse arrangement. The OPV/Bus Wire interface resistance is 32 mΩ at the start of pulse 1. The intent of this pulse is to break down any oxide on the wire surfaces at the interface. Note that the interface resistance at the start of pulse 2 is much less, 14.9 mΩ. Thus, pulse 2 does not have to break down the oxide layer as well as do the welding. As stated above, pulse 1 is in the current mode, where the maximum current is set. Pulse 2 is in the power mode, where the maximum delivered power is set. This difference is also important for proper welding.

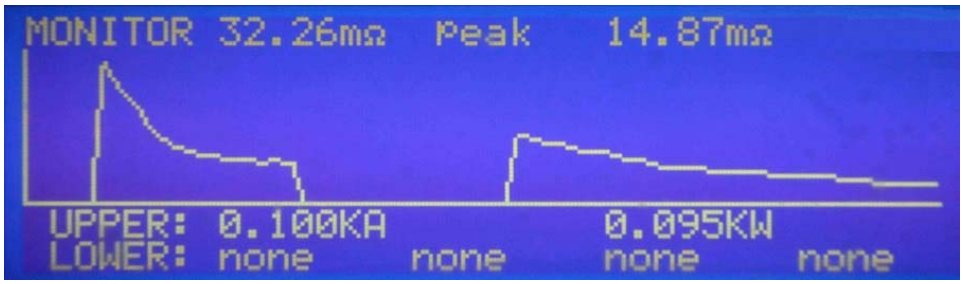

Figure 21: Interface resistance for a typical weld operation

Automated Welding

A prototype system was developed to demonstrate that the OPV wires protruding from the edge of a fabric can be automatically welded to the bus wires. A programmable X-Y table was used to move the fabric and align the OPV wires with the two bus wires. Motion of the X-Y table is controlled by a PLC connected to the table motors.

A vision system described above, and connected to the PLC, is used to identify primary and secondary OPV wires and signal the PLC when a wire is positioned between the welder heads. The PLC uses this information to activate the welder unit and weld the identified wire to one of the bus wires.

Figure 22 shows the vision system screen with a primary OPV wire aligned over the lower welder electrode. The bus wire is also positioned over the welder electrode and below the OPV wire. The green rectangles in Figure 22 are some of the vision system tools that identify the wire and determine if it is a primary or secondary wire. The PLC uses this information to stop the X-Y table with the wire in the proper position and then activates the welder controller to initiate and complete a weld operation.

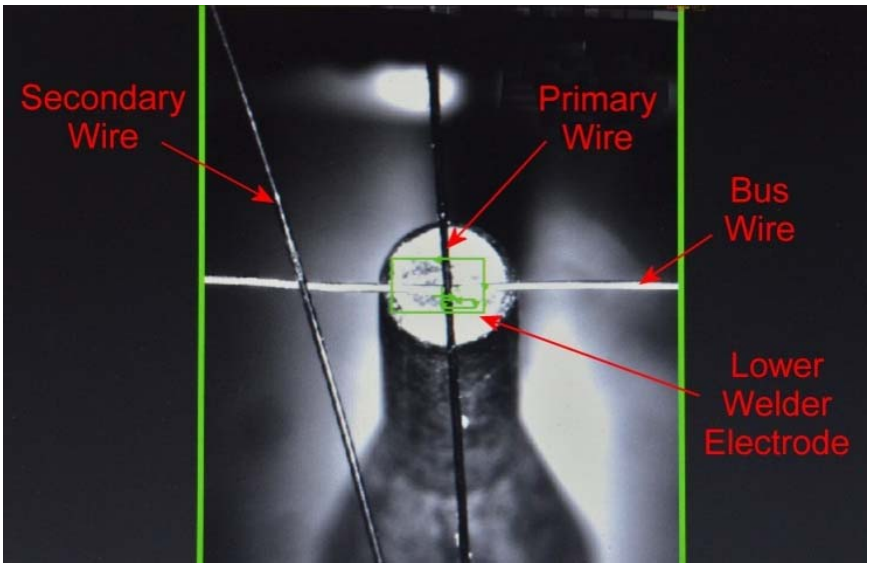

Figure 22. Vision system screen with a Primary OPV wire in place for welding

Figure 23 shows the upper welder electrode in place, pressing the OPV wire and bus wire onto the lower electrode at a controlled force. Electric current is flowing through the electrodes, welding the two wires together. During this operation the X-Y table is stationary. After the weld operation is completed the upper electrode moves back to its holding position and the X-Y table is activated, moving to the next wire to be welded.

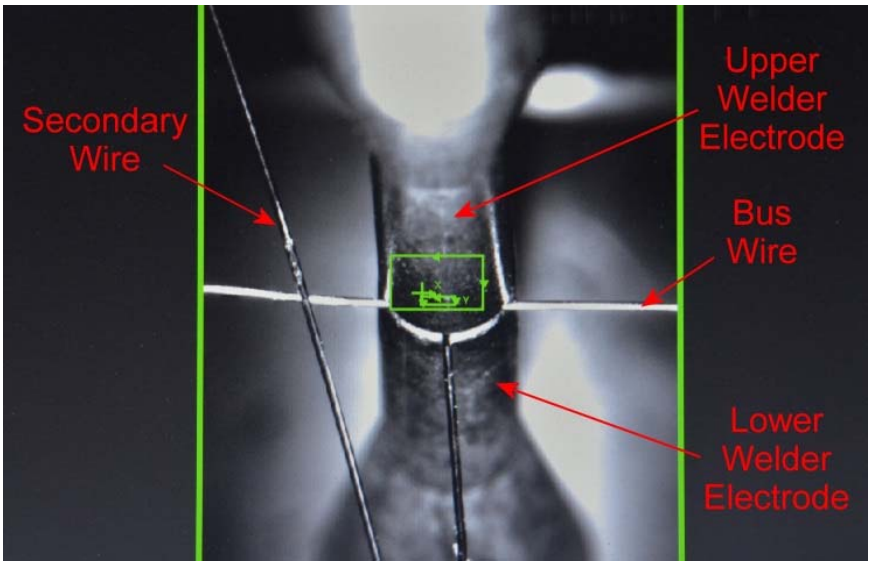

Figure 23. Vision system screen with the welder electrodes together performing a weld operation

Figure 24 shows two photographs of the actual welder electrodes. On the left, the electrodes are separated in their normal position and on the right, the upper electrode is in the welding position, pressing the OPV wire and bus wire onto the lower electrode.

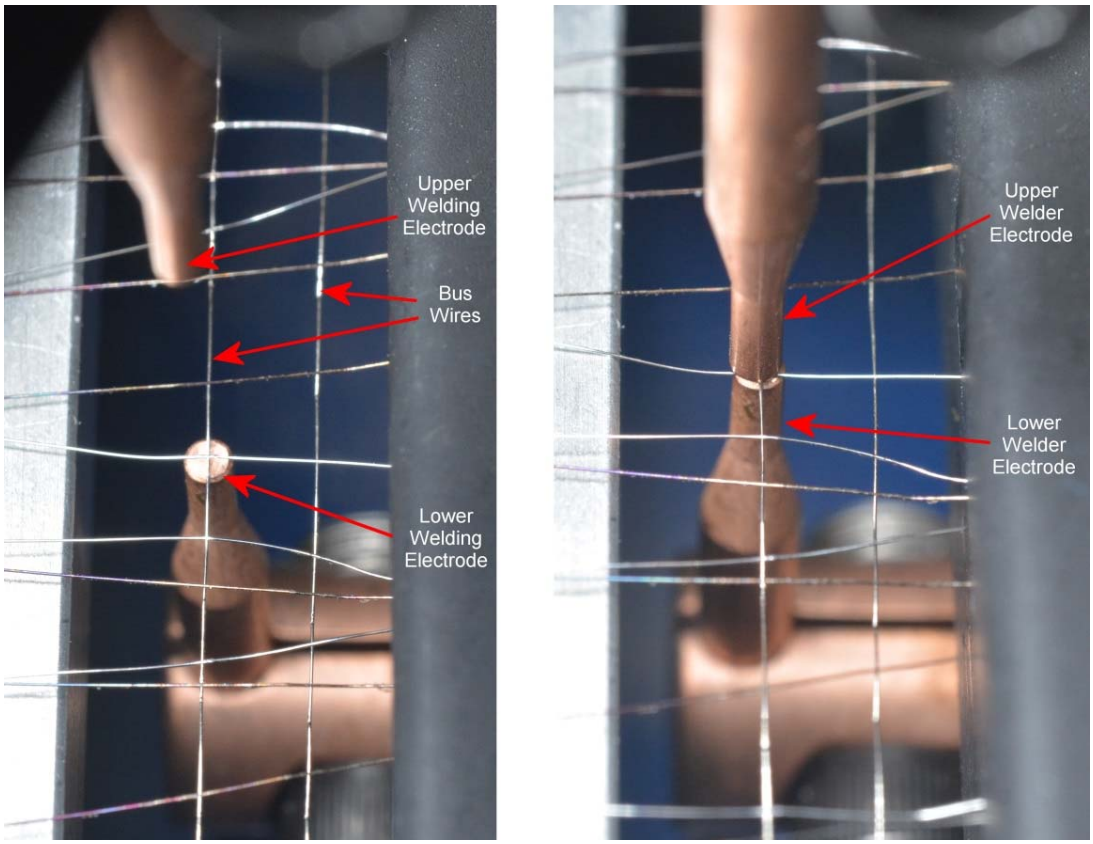

Figure 24. Photograph of the welder electrodes, both open and closed

During transition from one wire to the next, the movement of the OPV wires in the above photos is from top-to-bottom. The bus wire always travels above the lower electrode.

Figure 25 is a magnified view of the welded wires and is typical of the welds used in this program. This is not from an actual sample. Otherwise, the primary and secondary wires would not be welded to the same bus wire.

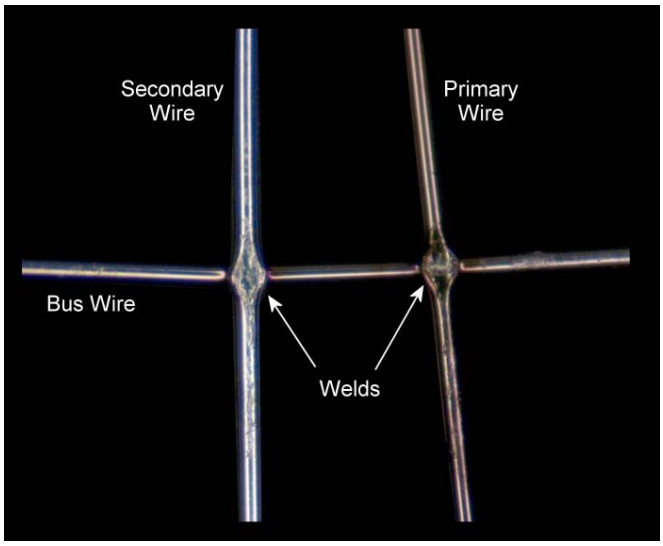

Figure 25. Microscope photo of the welded wires

Detailed Description of Results – Task 8

As indicated in the Task Summary section, the PV fibers presented a novel challenge to the weaving process. The mechanical properties of the PV wires did not allow us to convert them into a bi-directional PV fabric. We decided the fabrics would have PV wires only for the weft yarns and NYCO blended yarns (40/2 cotton count) for the warp yarns. Challenges in weaving preparation were solved by using a flat slab shuttle for PV wire insertion and a warping wheel for section beaming. We acquired a hand loom with a computer-controlled dobby for the fabric production. Thus, we did not experience problems that can be encountered with a mechanical shuttle loom such as loom tension, shuttle speed, winding tension, packing pressure, etc.

We developed a repeatable procedure of weaving PV fabrics through sectional warping and, with a few raddles as guides, the taping of yarns on a stick for tension control. Entering warp yarns through the heddles remained an undesired operation because it is time consuming, tedious and easily leads to errors. The approach we developed was to wind sectionally-warped yarns onto the rear beam of the loom, with the open ends taped on a stick placed above to (1) maintain the desired tension and (2) provide a sufficient length of yarns for entering. In Figure 26 (looking from the rear of the loom), part of the warp yarns have been entered, on the left side of the rear beam.

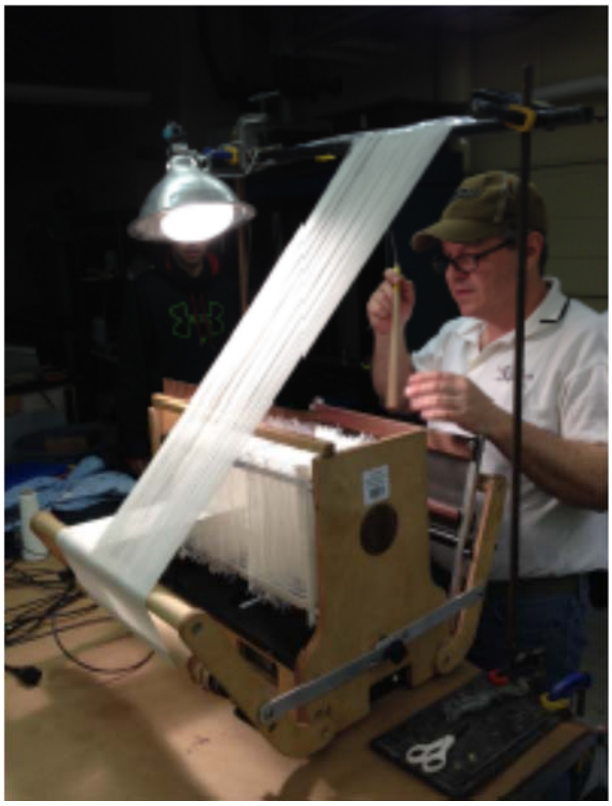

Figure 26. The new entering process

A group of warp yarns, typically nine, was then released from the stick and entered into the heddles with a hook. Figure 27 (a view from the front of the loom), shows this process after the first three have been entered and the next six remain to be entered. Every three yarns, after being entered into their corresponding heddles, were pulled forwards and entered into one slot of the reed located in the front.

Figure 27. A group of nine warp yarns (three of which have been entered) is released from the stick to be entered into the heddles.

After the entire group of 24 yarns was entered into a group of 24 heddles, the yarns were tied onto the front beam, the next group was started and the procedure was repeated until all 38 groups (38 x 24 = 912 yarns) were entered and tied. A small distance was kept between the heddles to allow easier visualization of the next group being entered (Figure 28).

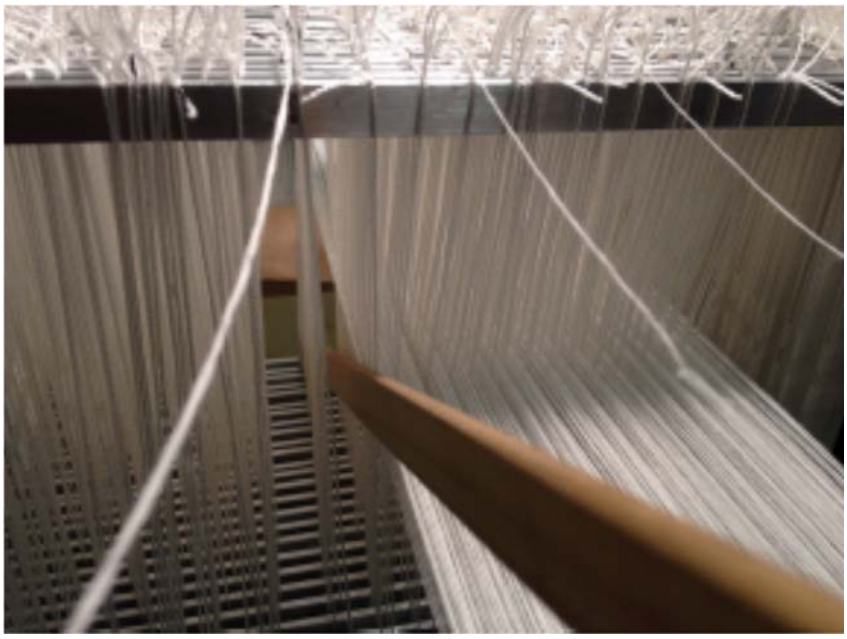

Figure 28. Heddles are separated from each other to increase the visibility of the currently engaged group and to minimize the possibility of mis-entering

Final Summary

This 1.5-year project demonstrated that high efficiency, flexible PV fibers can be produced in bulk and showed that they can be woven into effective energy-producing fabric panels. The fabrics are stiff in one direction but are flexible enough to be usable for flat areas of clothing or for non-clothing textiles such as backpacks and helmet covers. More studies need to be done for longer term properties and for function under practical conditions but we consider this effort to have been a great success.

This document reports research undertaken at the U.S. Army Natick Soldier Research, Development and Engineering Center, Natick, MA, and has been assigned No. NATICK/TR- 15/019 in a series of reports approved for publication.